A Probabilistic Risk Assessment Framework for the Path Planning of Safe Task-Aware UAS Operations

Uluhan Cem Kaya*, Atilla Dogan†, Manfred Huber‡
The University of Texas at Arlington, Arlington, TX, 76019, USA

This paper introduces a probabilistic risk assessment (PRA) framework for the path planning to quantify the risk of unmanned aircraft systems' (UAS) operations to the ground over populated areas. The proposed framework is designed to be flexible enough to address multiple concerns and objectives by utilizing the probabilistic risk exposure map (PREM) of the area of operation and UAS failure mode analysis with corresponding impact probability distributions on the ground. PREM is defined to be the risk of exposure of people or property on the ground to the presence of UAS in the air as a function of position, and it is used to model the distribution of risk exposure over the map. In this study, PREM is constructed for the impact related risk conditions where their distributions are modeled as a mixture of bivariate normal distributions over the discretized map of the area. Along with PREM, UAS failure modes with ground impact distributions are used in the derivation of the risk function to quantify the risk of being hit by the failing UAS platform for bystanders, properties and the traffic on the ground. Then, utilizing the derived risk function as a planning cost function, the path planner algorithm is used to plan a path that minimizes the risk according to the proposed risk assessment framework. As a path planner, optimal bidirectional rapidly-exploring random trees (RRT) is selected due to its fast convergence and optimality guarantee. Finally, the results of simulations for different scenarios are compared and discussed in detail.

I. Introduction

IN the past decades, unmanned aerial systems (UAS) have proved their usefulness in numerous civilian, commercial and military applications. Infrastructure inspections, environmental monitoring, delivery of goods, search and rescue missions, agriculture support and almost all military fields are just a few areas of these systems used among many other potential applications. Although there is a significantly increased demand for these systems, integration of UAS into the National Airspace System (NAS) has been relatively slow. For operating within NAS, an aircraft system must have comprehensive certification that satisfies rules and regulations set by the aviation authorities. Comparing the conventional manned aircraft systems current unmanned systems are lack of such documentation, and so, the reliability of these systems has not been fully assessed yet. Therefore, UAS operations in national airspace, especially over populated areas, presents a risk to people and property on the ground or other airspace users. Certainly, this situation raises safety, privacy and regulatory concerns. To benefit from the full potential of UAS, these concerns must be addressed systematically by defining and quantifying the risk conditions to these concerns so that acceptance of such technology by the society can be ensured. There is a great deal of work done on risk management strategies in the literature. These strategies mainly focus on modeling the risk itself as a product of hazardous event likelihood and the consequences of this hazardous event. Similarly, for the risk concept of UAS operations, several studies utilized the same strategy by developing a probabilistic model of the risk condition resulted from the operation of an unmanned vehicle over an area and analyzing the potential impacts of this risk condition, which is mostly done by casualty expectation due to vehicle impact to the ground. In Ref.[1], expected number of casualties is calculated for assessing the ground risk of railway inspection mission by

*Graduate Student, Mechanical and Aerospace Engineering, AIAA Student Member
†Associate Professor, Mechanical and Aerospace Engineering, AIAA Associate Fellow
‡Professor, Computer Science and Engineering

UAS by utilizing fault tree analysis of UAS and assuming ground impact points are distributed as a bivariate normal distribution over the maximum gliding range area. McGeer et al. presented gliding range model and impact location distribution as a probability density function to incorporate with probabilistic risk assessment (PRA) framework for finding potential harm to bystanders on the ground over populated areas in [2]. Similarly, various casualty expectations models due to mid-air collision and ground impact of UAS platform are developed in [3], [4], [5], and [6]. Also, Dalamagkidis et al. used the kinetic energy of the vehicle and shelter factor of the buildings in their expectation of casualties in [6]. The literature search showed that studies on the risk assessment of UAS operations made an approach to deal with only one of the concerns where the safety of bystanders is measured by the casualty expectation of UAS ground impact scenarios. However, although risk modeling of direct impact to bystanders on the ground plays a key role on public acceptance of UAS technology, a reliable and realistic risk assessment framework should consider all the potential risk conditions to address any concerns mentioned above. Thus, there is a need for more systematic risk assessment framework that can also incorporate the other risk conditions such as property damage, privacy violations, flying over restricted airspace or No Drone Flyover zones, in addition to the safety of bystanders.

In this research, a probabilistic risk assessment framework, which can be used to address aforementioned concerns, is presented for the quantification of risk exposure of UAS operations to the ground by introducing probabilistic risk exposure map (PREM) of the area of operation and using failure modes of UAS and their probability distributions of ground impact positions. PREM is defined to be the risk of exposure of people or property on the ground to the presence of UAS in the air, and it models the spatial distribution of the risk of exposure on the map. This concept is developed to integrate multiple objectives according to task characteristics, and by so, the task-awareness of the system is aimed. A similar concept is used in [7,8] for modeling threat exposure to UAS, which is opposite to how it is intended to be used here. Along with PREM, failure modes and their probability distributions of impact position on the ground are used in the derivation of the risk function for the risk quantification. After derivation of such function, path planners can utilize it to assess the risk of a mission (or task), and minimize the risk during the planning stage. In this study, due to its fast convergence rate and optimality guarantee, optimal bidirectional rapidly-exploring random trees (bi-RRT*) is selected to be used as the path planner with developed PRA framework. This approach is intended to be useful for decision making on UAS missions by assessing and comparing planned mission paths regarding their risk levels.

This paper is organized as follows. Section II describes the formulation of PREM and sample construction of PREM from building footprints. In Section III, UAS failure modes and derivation of ground impact distribution are explained and illustrated on the map. Proposed RRT algorithm and its pseudo code are introduced, and the integration of PREM with the failure modes and their ground impact distributions are formulated according to PRA framework in Section IV. In Section V, simulation results for different scenarios are displayed and discussed, and finally, the paper is concluded with a summary and the future works.

II. Construction of Probabilistic Risk Exposure Map

In literature, there are many studies on the risk analysis of UAS operations, especially over populated areas, using the expected number of casualties, injuries or people exposed to danger as a reasonable quantification unit of the risk assessment [1-6]. Therefore, population distribution (or the risk distribution) over the area of interest is required to be known in advance or modeled to assess the risk associated with the UAS operation. In this paper, distribution of the risk exposure is modeled using the PREM concept. PREM is defined to be the risk of exposure to the presence of UAS in the air, and it represents the distribution of risks as a function of position on the ground. To illustrate, considering human population on the ground, the higher population in a specific area that is subjected to UAS operation, the higher the risk of exposure (such as being hit by UAS or privacy violation) will be observed over that region. In this concept, the operation of UAS in urban areas is treated as a risk to the safety of bystanders, properties, and the other ground objects. Moreover, privacy and regulatory concerns regarding these operations can be addressed within the same concept. Thus, multiple objectives can be achieved by the PREM which consists of multiple layers corresponding to different types of risk classifications such as the risk of flying over people (or traffic), of flying closely over residential units, or of violating restricted airspace. The flexibility of the concept also allows fusing various risk layers into the same risk map. The advantage of having only one map is that once all the risk types are fused and included in the PREM, decision-making strategies do not need to distinguish

between different types of risks since the map already contains the required information.

Assume that a risk type is formed by the contribution of the individual risk sources of the same risk type, $\{S_1, S_2, ..., S_N\}$, where they are independently modeled and discretely placed across the map. Also, assume that evidences for this discrete risk mapping approach to represent the actual risk map is given with a binary random variable $M(e)$, where $e = \{e_1, e_2, ..., e_m\}$ are evidences. Under those assumptions, risk condition for this risk type in a particular location and time can be characterized by these two factors, namely **i)** the probability density of the risk condition R at location x and time t given the evidences of correct mapping $M(e)$, and an individual risk source S_j, $p(R(x,t)|M(e(t)), S(t) = S_j)$, and **ii)** the probability of given individual risk sources to capture total underlying risk condition given the $M(e)$, $P(S(t) = S_j|M(e(t))$. Basically, the first term represents the spatial and temporal distribution of the risk condition caused by the given risk source as a probability density function, while the second term models fraction of underlying risk condition captured by the individual risk source S_j. By the product of these two factors, the probability distribution of the i^{th} type risk condition for a given set of evidences can be constructed as

$$p(R^i(x,t)|M^i(e(t))) = \sum_{j=1}^{N} \Big[p(R^i(x,t)|M^i(e(t)), S^i(t) = S^i_j)\Big]\Big[P(S^i(t) = S^i_j|M^i(e(t)))\Big] \tag{1}$$

where N is the total number of discrete risk sources.

In addition, conditioning on $M(e(t))$ in Eq.(1) can be eliminated by utilizing the probability of risk mapping for the given set of evidences to represent actual risk mapping. This term introduces the uncertainty into the PREM concept, and it can referred as a situational-awareness of the system. By this approach, a priori knowledge about the environment and the risk conditions can be updated as the new information gained, or the evidences collected, by any means.

$$PREM^i: \quad p(R^i(x,t)) = \sum_{M\in\{T,F\}} \Big[p(R^i(x,t)|M^i(e(t)))\Big]\Big[P(M^i(e(t)))\Big] \tag{2}$$

where T and F are the true/false. Note that Eqs.(1-2) are generic equations to model PREM. However, time dependency of the underlying process and the uncertainty on the correct identification of the risk mapping are out of scope for this study. Therefore, the underlying risk condition is assumed to be stationary, and uncertainty on the modeling is neglected ($P(M(e) = True) = 1$).

$$PREM^i: \quad p(R^i(x)) = \sum_{j=1}^{N} p(R^i(x)|S^i = S^i_j(l_j, m_j))P(S^i = S^i_j(l_j, m_j)) \tag{3}$$

where l_j is the location of the center of the individual risk source, and m_j is the modeling parameter of the risk distribution for this risk source. Each risk sources is identified by these two parameters. This approach gives us the flexibility to model the total risk distribution as a mixture of distributions over the discrete set of locations.

Furthermore, multiple risk types can be integrated into the same risk map with this approach by assigning weight factors for each risk types according to their importance. Note that, accumulation of the different risk types over a trajectory might differ from each other. One clear example is that while the privacy risks might be purely depending on the current location of the UAS and accumulated over time, UAS platform impact related risks would require where the platform failed and what the state of the vehicle was at the failure as well. Therefore, one should differentiate the dissimilar risk types during fusing. Nevertheless, one risk map fusing all the similar risk types(layers) can be formulated as below

$$p(R(x)) = \sum_{i\in\{a,b,...\}} w^i p(R^i(x)) \quad \text{or} \quad PREM = \sum_{i\in\{a,b,...\}} w^i PREM^i \tag{4}$$

where w^i is the weighting of the risk type i and with the condition of $\forall i : w^i \geq 0$, $\sum_i w^i = 1$.

Another advantage of fusing multiple risk types in this approach is that every UAS mission may impose a different set of weights on various risk conditions. For instance, weight on the privacy risk of residences would differ widely from a UAS executing the task of pizza delivery to transferring a live organ transplant task. By this approach, only changing weights w^i in Eq.(4), task-awareness of the system can be achieved, even during task execution.

Lastly, benefits or opportunities present in the environment, which are separate from task objectives, can be captured as well in this context by seeing them as negative risks. This approach can be useful in a variety of task and help decision-making strategies.

In this paper, derivation of Eq.(3) is explained as an example for only one risk type, which is a impact related risk condition. Exposure of buildings to a UAS over an area is selected as a risk condition. PREM is modeled using the building footprints in a specific area, taken from geographical information system (GIS) database. Also, the distribution of the risk condition is characterized by the mixture of Gaussian probability density functions (PDFs) such that the mean of each PDF represents the concentration point (location) of the risk condition and the standard deviation of the PDF represents how far the risk condition spreads out (modeling parameter). For a two-dimensional map, bivariate Gaussian PDF is used as follows

$$f(\mathbf{r}) = \frac{1}{2\pi\sqrt{det(\mathbf{K})}} \exp[-\frac{1}{2}(\mathbf{r}-\mu)^T\mathbf{K}^{-1}(\mathbf{r}-\mu)] \tag{5}$$

where $\mu = [\mu_x \ \mu_y]^T$ and $\mathbf{K} = diag\{\sigma_x^2, \sigma_y^2\}$ are the mean vector and the covariance matrix of the PDF and $\mathbf{r} = [x \ y]^T$ is the position vector.

The mixture can be thought as the sum of 'bumps' located across the area representing the spatial and quantitative distribution of the risk condition. The higher the risk density is, the higher the bump will be observed. In this stage, one can assign a Gaussian PDF for each building (or people) to model the risk distribution. However, to obtain a tractable system and to reduce the computational complexity on larger scale applications, the whole map is discretized into smaller grids so that multiple buildings falling into the same grid can be represented by one PDF, that might be seen as the trade-off between precision and tractability. In this approach, each grid can have only one Gaussian PDF located at the center of the grid, which is defined by l_j in Eq.(3). The dimension of the grid defines how far the the risk condition spreads out, which is in terms of the standard deviation of Gaussian PDF and represented by the modeling parameter m_j. After selecting a grid size, the standard deviation of the PDFs is parameterized in terms of the selected grid size to fit the effective area of PDF, which is determined to be 1.1-σ deviation from the mean, inside the grid boundaries, and used as a constant for all the PDFs. Yet, by this approach, all of the grids have the same PDF although they may have a different number of buildings or even do not have any. What's more, during the construction of PREM, grids having the denser population should have a higher risk of exposure than the grids with lower population densities. To address these points, a weighted sum of Gaussian PDFs is introduced with the second term in Eq.(3) by using fraction of total risk condition in each grid as the weights. Building densities in each grid are used as fractions, and they are computed by assigning center of each building to corresponding grids and dividing the number of buildings in the current grid by the total number of buildings in the map. It means a building can be accounted for only one grid even though it might fall into multiple grids. This approach can be easily improved using additional methods, but it is not intended in this study since it is not the primary goal. Fractions are denoted as $\pi(S_j(l_j, m_j))$ in Eq.(6) instead of $P(S^i = S_j^i(l_j, m_j))$. Construction of PREM with weighted sum of Gaussian PDFs is below.

$$PREM(\mathbf{r}) = \sum_{j=1}^{N_{pdf}} \pi(S_j(l_j, m_j)) \frac{1}{2\pi\sqrt{det(\mathbf{K_j})}} \exp[-\frac{1}{2}(\mathbf{r}-\mu_j)^T\mathbf{K_j}^{-1}(\mathbf{r}-\mu_j)] \tag{6}$$

where $\mu_j = l_j = [l_{x_j} \ l_{y_j}]^T$ and $\mathbf{K_j} = diag\{\sigma_{x_j}^2, \sigma_{y_j}^2\}$. N_{pdf} is the total number of PDFs in the map.

Also note that, selection of grid size during the discretization of the map plays an important role in the estimation of actual risk distribution. If the selected grid size is too small, the estimation will be a sum of isolated bumps of PDFs which means risk conditions are restricted to stay in small isolated areas. Conversely, if a large grid size is selected, densities (bumps) will cover vast areas individually, and this might result in spending too much effort on the areas where no risk has been observed. In addition to the true representation of risk distribution, a minimum resolution that path planning is required needs to be considered for selection of an appropriate size of the grid.

An example of PREM is shown in Fig.(1). Figure on the left is two-dimensional contour plot of PREM constructed from building footprints on an area where the small red blocks represent the buildings, and the isolines show decreasing PREM values from inside to outside. Figure on the right is the three-dimensional surface plot of the same PREM.

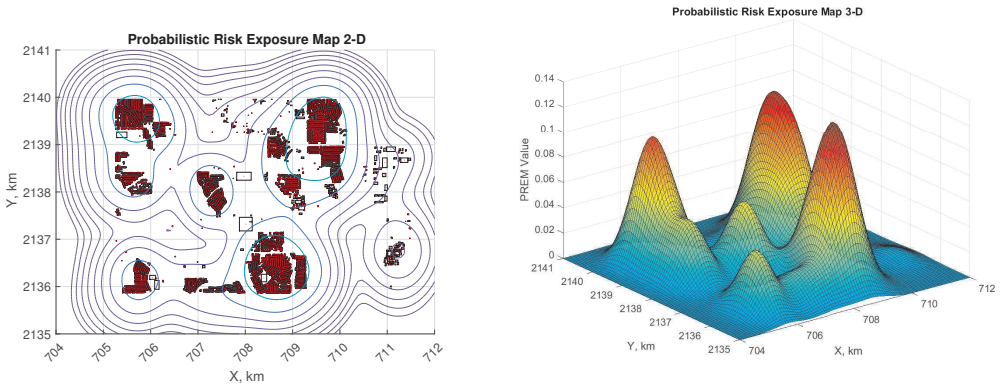

(a) PREM in 2D Contour Plot

(b) PREM in 3D Surface Plot

Figure 1. Illustration of a sample PREM

III. UAS Failure Modes and Ground Impact Distribution

In this section, failure modes of UAS and their ground impact probability distributions over the map are investigated briefly, and a simple example is illustrated. Modeling the actual behavior of an unmanned aircraft system under critical failure conditions is not trivial due to the inherent nature of the operating environment and non-linearity of vehicle dynamics. There is a considerable amount of work done on this topic to identify the possible behaviors and to assess the reliability of these systems. As with the fault tree analysis,[9] failure mode analysis is one of the common methods to model the resulting behavior of the system under certain failure conditions, which are called failure modes. Failure occurring on an aircraft system can result in two operational conditions, namely controllable flight and uncontrollable flight. While the normal mission can still be maintained or mitigation strategies can be performed in a controllable flight, in an uncontrollable flight, the mission is terminated by the loss of control on the system with a potential crash scenario. In this work, all the failure modes are presumed to result in an uncontrollable flight, and no mitigation strategies are performed. Resulting behavior of the UAS after a failure is analyzed regarding the impact location distribution over an area on the ground. Impact location is defined to be that in an uncontrollable flight condition, a position on the ground that UAS can reach from its current state where the failure occurs. Impact domain of UAS is represented by a probability distribution over the map for a given uncontrollable flight condition UF occurred at current state of the vehicle $X(t)$, and at current environmental conditions $e(t)$, $f(ImpPos|UF(X(t), e(t))$. Domain depends on the capabilities of the vehicle such as operating speed and available power on-board, and environmental conditions like wind direction and magnitude. The range and endurance of the UAS can be significantly altered by the presence of strong weather conditions. Therefore, environmental conditions should be considered to determine the size and shape of the impact domain. Also, in case of diminished capability modes such as a sensor, actuator or system unit failures, the range or endurance will be adversely affected. This approach can be used to determine probability density of impact locations over the map under each possible failure case according to their occurrence probabilities, and the mixture of these distributions will provide the probability distribution of impact locations for all failure modes over the map. As it is explained in Section II, impact probability distribution of all failure modes is formulated as a mixture distribution. Eq.(7) shows the formulation of mixture distribution.

$$f(ImpPos|UF(X(t), e(t))) = \sum_{j=1}^{k} \Big[f(ImpPos|F_j, UF(X(t), e(t)))\Big] \Big[P(F_j|UF(X(t), e(t)))\Big] \tag{7}$$

where $f(ImpPos|F_j, UF(X(t), e(t)))$ is the probability density function that represents UAS ground impact probability distribution over the map given that uncontrollable flight UF is caused by the jth failure mode F_j, at the current state of UAS, $X(t)$, and environmental conditions $e(t)$. $P(F_j|UF(X(t), e(t)))$ is the conditional probability of the jth failure mode to cause uncontrollable flight at given conditions among all failure modes. Also, k is the total number of UAS failure modes.

Note that, the occurrence of failure modes can depend on many factors. Hence, current vehicle states, environmental conditions and time are included in conditional probabilities to address some of those factors. Using mixture distribution, the probability of UAS impact to a particular area A given a failure happened at a specific state and condition can be obtained by below integral.

$$P(ImpArea(A)|UF(X(t),e(t))) = \iint_A f(ImpPos(x,y)|UF(X(t),e(t)))\,dx\,dy \tag{8}$$

In addition, considering the density of uncontrollable flight condition to occur at a given specific vehicle state and environmental conditions $\lambda_{UF}(X(t),e(t))$, $UF(X(t),e(t))$ term can be eliminated from the condition in Eq.(8).Then, UAS impact density to an area A can be obtained given the current time as

$$\lambda_{ImpArea}(A,t) = \lambda_{UF}(X(t),e(t))P(ImpArea(A)|UF(X(t),e(t))) \tag{9}$$

Note that, the reason why density of uncontrollable flight condition is used instead of probability is because for any exact $X(t)$ and $e(t)$, the probability of observing UF is zero since it is a continuous random process. $\lambda_{UF}(X(t),e(t))$ models the effect of time varying vehicle states and environmental conditions on uncontrollable flight condition occurrences.

In this paper, to convey the proposed idea clearly, failure modes and their impact probability distributions are overly simplified with specified constant failure rates and uniformly distributed ground impact position probabilities over constant elliptical regions on the map. Also, environmental conditions are not taken into account. An example is illustrated in Fig.(2). In this example, three different failure modes, depicted by different colors for a UAS located at (1,1), are defined with constant elliptical impact regions. For each failure modes, the probability density of impact locations is chosen to be a uniform distribution. It means that given the failure mode, every position on its defined domain has the same impact density, which is of course not the real case for any flying vehicle. In Fig.(2(a)), green region, denoted by F_1, is the first failure mode defined by larger impact domain with 0.5 occurrence probability given a failure occurred, $P(F_1|UF(X(t),e(t)))$. Since it has the largest area compared to the others, probability density function, $f(ImpPos|F_1,UF(X(t),e(t)))$, has the lowest height. For the second failure mode, denoted by F_2 and yellow color, shape and size of the distribution is altered and relative occurrence probability is chosen to be 0.3. The red region, denoted by F_3, is the last failure mode with the smallest impact area with relative occurrence probability of 0.2. In Fig.(2(b)), result of Eq.(7) is plotted. Plot represents the combined ground impact probability distribution of all failure modes. As it is expected, the intersection of all failure mode regions has the highest density. In this example, failure occurrence probabilities, impact domains and their distributions are intentionally selected to be simple. However, the effect of weather conditions, diminished capabilities and the other parameters can be modeled as probability density functions over the map. Thus, Eq.(7) can easily be constructed for more complex scenarios.

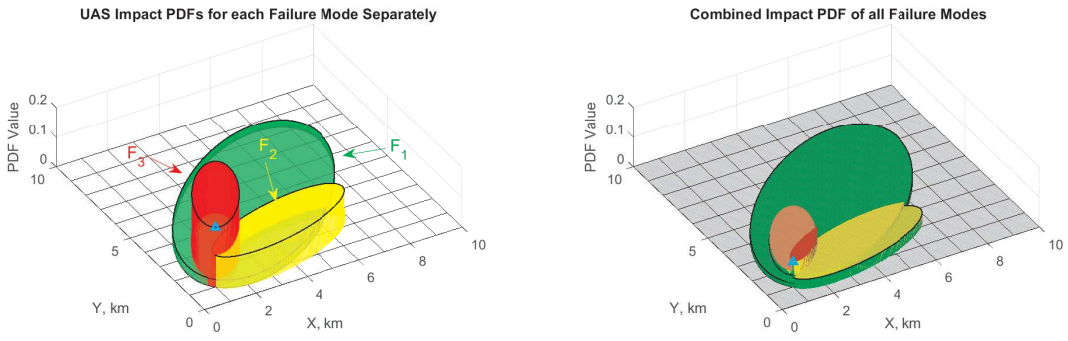

(a) Isometric View of Ground Impact PDFs

(b) Isometric View of Combined Impact PDF

Figure 2. Illustration of a sample UAS ground impact probability distribution for three failure modes

IV. RRT Path Planner with Probabilistic Risk Assessment

During the path planning stage, probabilistic risk assessment is introduced to find the total risk (or cost) of following a path by integrating previously defined PREM and UAS impact probability distribution in a systematic framework for efficient use of path planner. Therefore, as in the case of real world UAS operations, exposure of the risk, dynamically changing environment and the vehicles capabilities and characteristics can be taken into account for a safe and successful mission planning. After deriving the cost function, expected cost of a path can be optimized by the path planners. In this study, it is proposed to use modified optimal bidirectional rapidly-exploring random trees (RRT) that utilizes PREM and failure mode analysis to efficiently expand trees to find potential paths while estimating their expected costs with the goal of incrementally optimizing the cost of trajectory. In addition, RRTs can be used to explore the whole map continuously while maintaining tree structure so that given the destination point, it is guaranteed to find the path with optimum utility measure as the number of samples approaches infinity. Although convergence is guaranteed at the infinity, given the appropriate heuristics for searching optimum trajectory cost, RRTs can generate the path in acceptable optimality range and time limits.

A. RRT Path Planner

Sampling-based planners such as RRT and PRM (Probabilistic Road Map) have been used for many motion planning problems and shown to be probabilistically complete and computationally efficient. Many variants of the RRT algorithm have been derived and successfully applied to complex motion planning problems. One of them is the bidirectional RRTs which are often applied to planning problems with challenging regions or high-dimensional configuration spaces with numerous obstacles, and it is observed to show fast convergence on these problems. Another variant of the RRT algorithm - RRT* that provides asymptotically optimal solutions, has been presented and investigated by Karaman in Ref. [10]. In Ref. [11], examining previous variants of RRT algorithm, simple bidirectional RRT* has been introduced.

In this paper, a slightly modified version of bidirectional RRT* with a goal biased heuristic will be used for path planning. The Pseudo code of the algorithm is outlined in Algorithm (1) Appendix A. There are two tree structures maintained, one of them originating from the initial position and the other one from the goal position. These are denoted as T_1 and T_2 respectively. The algorithm requires initial configuration, x_{init}, and goal configuration, x_{goal}, maximum sampling iteration number, IterMax, probability of goal bias, P_{goal}, probability of second tree to attempt for a connection, $P_{connect}$, and distance threshold for connecting two trees' nodes, Threshold, as inputs of algorithm, and it generates the path segments, E_{path}, risk of the path, r_{path}, nodes of the path, σ_{path} and two trees as outputs. In line 1 and 2, nodes, path segments and trees are initialized. Algorithm starts with selecting a new configuration x_{rand}, finding the nearest node of T_1 to x_{rand} and extending a branch from $x_{nearest}$ to x_{rand} (Lines 4-10). Extended new node, x_{new} is checked by the collision check algorithm, CollCheck. If no collision is present, the risk of extending a new branch, r_{new}, is calculated, and path segments and nodes are updated (Lines 11-14). In Line 15, the set X_{near} of all nodes that are close to x_{new} on the first tree is found, and Rewire function in Algorithm (2) Appendix A checks the possible improvements of using the other pathways along near nodes according to defined risk metric in Line 17. If there is any, path segments and the parents of tree branches are updated. Rewiring details can be found in Algorithm (2) Appendix A. For the second tree, above process is slightly altered so that instead of goal probability bias, P_{goal}, probability bias of connecting T_2 to a newly extended branch of T_1, $P_{connection}$, is used. After extending branches of both trees, whether the path segments of two trees are connected or not is checked (Line 33), and if there is any connection, using path segments of both trees and connection nodes, Backtrack function generates the output of the algorithm (Line 34). This process is repeated until the maximum iteration number is reached, and then, the path with minimum risk is chosen as the final path.

In the above algorithm, risk function to calculate the risk of nodes and path segments is derived in the following section.

B. Probabilistic Risk Assessment

In this section, probabilistic risk assessment is defined to quantify the risk exposure of UAS operations to the ground. There are a few scenarios that a risk condition can arise due to these operations. The obvious one is the crash scenarios of the platform or uncontrolled deviation of its planned trajectory such that it can pose

a threat. These scenarios are categorized as event-based risk conditions in this paper. However, there are other scenarios causing risk conditions that are not event-based such as privacy intrusions. This category has not been fully defined yet, and it is still an open debate. Therefore, the proposed risk assessment framework is modeled for only the event-based risk conditions, more specifically for the events causing platform impacts to the ground. Nonetheless, the flexibility of the previously introduced concepts and extensibility of below framework can easily allow us to cover the other abovementioned scenarios as well. This study utilizes the risk exposure map of the area considering UAS failure modes and their ground impact probability distributions to quantify the risk of UAS platform impact risk to the ground, where buildings and stationary traffic are subjected to this risk condition. First, time parameterized density of the risk condition is derived in Eq.(12) along the UAS trajectory. Then, the total risk of UAS impact along the path is formulated as the integration of risk densities and event probabilities with respect to time in Eq.(14). Finally, derived equation in Eq.(14) is used as the risk function (or cost) of the path planner in Algorithm (1).

Eq.(10) describes the calculation of uncontrollable UAS flight condition risk to an area A given that this flight condition is occurred at current state of the vehicle, X and environmental conditions, e at time t. Basically, given the information where and when the UAS failed, impact risk on the ground is estimated by using the spatial distribution of impact probabilities and the expected value of the total risk condition on the impact area as

$$Risk(\text{area } A \text{ given } UF(X(t), e(t))) = Pr(\text{Impact to area } A \text{ given UF at X(t) and e(t))} \times [\text{Risk on } A] \quad (10)$$

Using the above relation, risk values of the elementary (or grid) areas can be calculated for a given UF condition. Assuming that UAS failure modes and their impact distributions over the map are constructed with uniform impact distributions on constant circular impact domains, shown as colored nested circular regions around yellow triangle mark in the center of Fig.(3(a)) where yellow triangle depicts the position of the platform when failure occurred, Fig.(3) illustrates the integration of a sample PREM and failure modes' ground impact distributions. Fig.(3(b)) show the result of Eq.(10) for each one of the individual grid areas. As it can be seen, risk on the grids where impact domains intersect with high-risk regions have higher expected impact risk. Also, note that, outside of the impact domains, there is no risk expected since those regions are not reachable by the failing vehicle. Furthermore, total corresponding risk for this condition can be obtained by the summation of all individual risk elements as $\sum_{A_i \in A_F} Risk(A_i | UF(X(t), e(t)))$, where A_i and A_F are the grid area and total area enclosing all the failure mode domains.

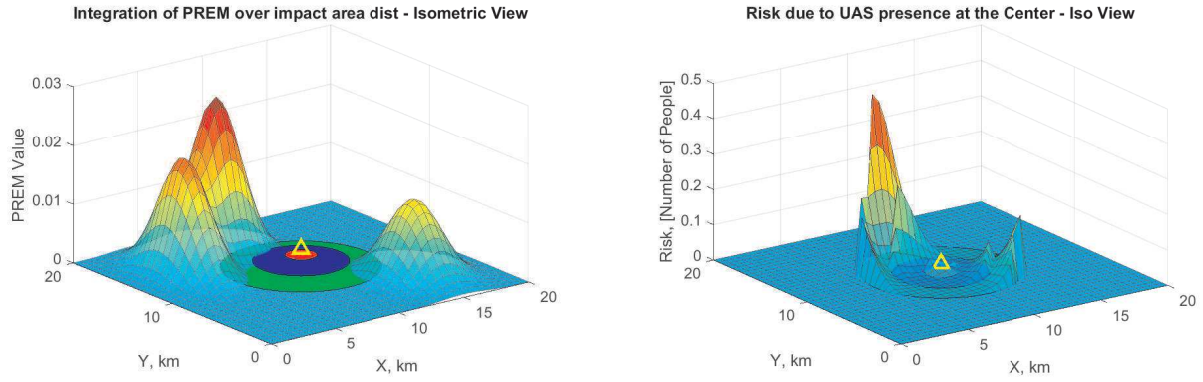

(a) Integration of PREM and Failure Modes

(b) Risk on Grid Areas due to UAS at the Center

Figure 3. Illustration of PREM and failure mode ground impact distribution integration

Eq.(10) requires the uncontrollable flight condition to be known in advance to compute the risk for an area. On the other hand, employing UAS impact density, introduced in Eq.(9), the occurrence rate of the UF condition can be included in the risk calculation. By so, impact risk density to ground caused by the presence of a UAS at a specific state and environmental condition can be expressed as follows

$$RiskDensity(t) = \sum_{A_i \in A_F} \lambda_{ImpArea}(A_i, t) \times [\text{Risk on } A_i] \quad (11)$$

Impact density and expected total risk on the elementary area A_i are shown in the formulation of risk density in Eq.(12). Impact density to area A_i is found by multiplying density of having uncontrollable flight occurring at $X(t)$ and $e(t)$ by the integral of the conditional impact probability distribution of UAS given UF occurred at given conditions. Similarly expected total risk over the area A_i is found by integrating PREM over the elementary area. Then, this calculation is repeated for each elementary areas inside the union of all impact domains, denoted by A_F, on the map. The calculation in Eq.(12) is unit-less in this form. However, if PREM has a quantitative measure for corresponding risk condition, such as the number of people, then it can be used as a unit with impact density unit, which is usually defined with flight hours.

$$RiskDensity(t) = \sum_{A_i \in A_F} \Big[\lambda_{UF}(X(t), e(t)) \iint_{A_i} f(ImpPos(x,y)|UF(X(t),e(t)))\, dx\, dy\Big]\Big[\iint_{A_i} PREM(x,y)\, dx\, dy\Big] \tag{12}$$

Using the formula derived in Eq.(12), risk level of the path can be computed by integrating the impact risk densities along the path. However, this integration implies that failure is assumed to be occurring in every time step. This assumption is not correct. Because after the first failure case, vehicle cannot proceed the normal operation, and so, the risk that corresponds to the remaining part of the path, after the failure occurred, cannot be included in total risk. For correct integration of total risk, the probability of not having any failure in a given time period should be known until reaching the goal. Also, this probability term can be seen as a discounting factor in Eq.(13). It means that the risk in the near future has a higher weight (or importance) than the risk in distant future during the risk calculation.

$$Risk = \int_0^{T_{Path}} P(\neg UF(X(t), e(t)))RiskDensity(t)\, dt \tag{13}$$

where T_{Path} is the total elapsed time until UAS to reach its destination. $P(\neg UF(X(t), e(t)))$ is the probability that no failure occurred until time t.

If failure modes are assumed to be following a Poisson distribution with constant failure rates, Eq.(13) can be reconstructed as

$$Risk = \int_0^{T_{Path}} e^{-\lambda t} RiskDensity(t)\, dt \tag{14}$$

where $\lambda = \sum_j \lambda_j$ is the summation of individual failure mode rates following Poisson distribution. Note that, Poisson distribution with zero event has exponential decay ($P(X(t) = 0) = e^{-\lambda t}((\lambda t)^0)/0!$).

Eq.(13) is basically in the form of performance index as below.

$$J = \psi(x(t_f), t_f) + \int_0^{t_f} L(t, x, u)\, dt$$

where t_f is the final time of the solution, and the first term represents the cost of the final state of the solution. $L(t, x, u)$ function is used to account for the cost of following a specific trajectory such as total distance traveled or the duration. It is selected to be the total risk of following a path with the term inside the integral in Eq.(13) for this study. Final state constraint is not considered.

In this study, risk levels of the planned paths will be used to compare different paths. Therefore, the main purpose of the path planner is to minimize the risk along the path in Eq.(14). Fig.(4) illustrates the calculation of the risk for a sample RRT generated path in 20 km by 20 km map. Three failure modes are specified with constant failure rates of 10^{-4}, 10^{-2} and 10^{-1} per hour respectively, and circular impact domains with radius of 1 km, 0.8 km and 0.6 km. In Fig.(4(a)), red line describes the actual path of UAS planned by RRT planner from initial position marked with a red square on the bottom left to goal position marked with a green triangle on the upper right corner. The other black lines are the branches of the tree created by RRT. To find the total impact risk along the path, Eq.(14) is used, and the result is shown in Fig.(4(b)).

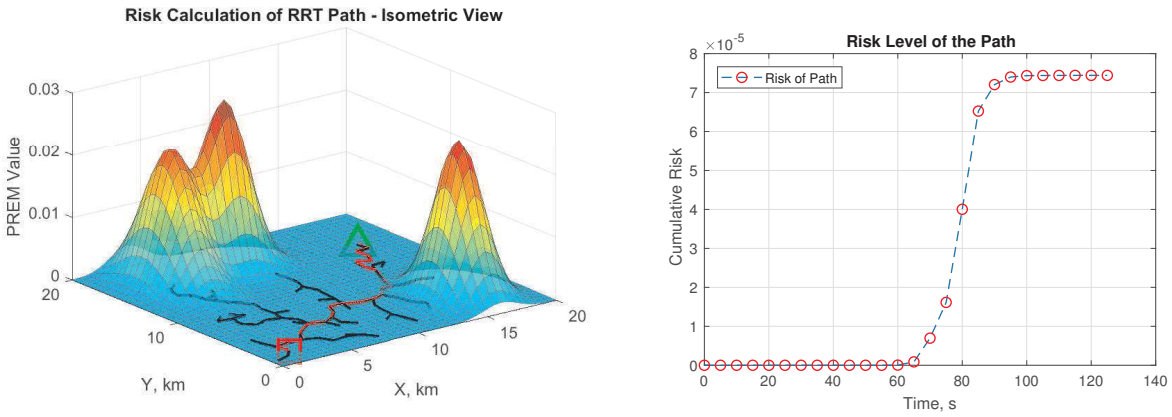

(a) Isometric View of RRT Path

(b) Risk Level of the Path

Figure 4. Illustration of a sample risk calculation on the RRT Path

V. Results of Simulations

In this section, the proposed probabilistic risk assessment framework is implemented in two different scenarios, and the obtained results are discussed. Implementation consists of 4 steps; construction of PREM layers from the data such as building footprints and road layout of the selected area, defining failure modes with corresponding failure rates and their ground impact probability distributions, selection of required parameters for the RRT path planner such as step size and goal bias, and finally, generation of the path between selected positions by utilizing the risk assessment. In the last step, the path planner algorithm runs until the maximum number of iterations is reached. Assuming that algorithm finds a path before reaching the maximum iterations, for the remaining iterations, alternative paths with the lower risk levels are searched since asymptotically optimal paths are guaranteed iteratively by bidirectional RRT* algorithm. In the end, risk levels of all the paths found incrementally are saved, and the path with the lowest risk level is chosen to be the final path of UAS. The final path and previously found paths are shown in the same graph for comparison with respect to their total path lengths and total risk levels.

In this study, failure modes and their ground impact probability distributions are defined for both scenarios and used as the same. Four failure modes with constant failure rates, which follow the Poisson process, and with constant elliptical impact domains, as shown in Fig.(5(a)), are determined for the UAS. Table 1 lists the failure mode parameters. Impact distributions are modeled with truncated Gaussian PDFs such that 3σ deviation of the Gaussian falls within the corresponding impact domain. Combined ground impact probability distribution is shown in Fig.(5(b)). Note that, the orientation of the impact domain is with respect to the body frame of the platform, and it rotates with that.

Table 1. Failure Mode Parameters

Failure Modes	Failure Rates	Impact Domain Shape	Orientation
F_1	10^{-5} per hour	Ellipse (50 m x 33 m)	$\angle 0°$
F_2	10^{-4} per hour	Ellipse (37 m x 21 m)	$\angle$-30°
F_3	10^{-3} per hour	Ellipse (33 m x 16 m)	$\angle 0°$
F_4	10^{-4} per hour	Ellipse (37 m x 21 m)	$\angle 30°$

Parameters that the RRT algorithm requires are listed in Table 2 for both scenarios. Maximum iteration number for the run is determined to be 10000. However, the longer it runs, the more optimized solution can be obtained. The speed of the vehicle is chosen to be 20 km/h with a step size of 5.5 meters, which is the distance vehicle travels in 1 second. Goal bias of 0.01 for exploring the regions near the goal position and the connection bias of 0.02 for connecting two trees each other are used.

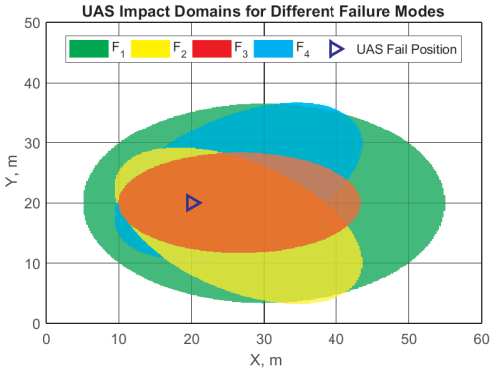

(a) Impact domains of failure modes - separately

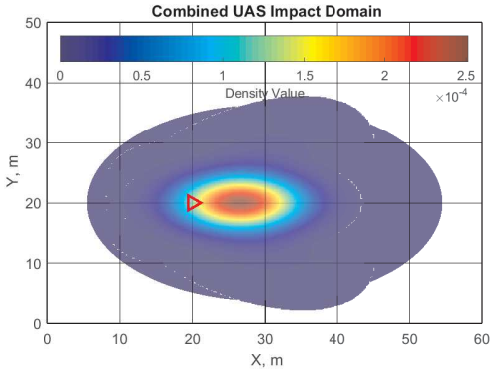

(b) Combined ground impact probability distribution

Figure 5. Failure mode impact domains and combined ground impact probability distribution

Table 2. RRT Parameters

V	20 km/h	**Step Size**	5.5 m	P_{goal}	0.01
IterMax	10000	**Threshold**	0.4× StepSize	$P_{connect}$	0.02

A. First Scenario

In this scenario, a small residential area with a rectangular dimension of 400 by 400 meters is selected as the UAS operation area in Fort Worth, TX. For this region, PREM is constructed for the risk of flying over properties and traffic, which is assumed to be stationary. Therefore, the risk of being hit by the UAS for the properties and the vehicles will be considered by the risk assessment framework. Two cases are investigated in this scenario to compare the results. In the first case, shown in Fig.(6(a), only the property risk exposure are present in the environment (late night UAS operation). In Fig.(6(b)), the second case includes both property and traffic risk exposures for the risk assessment (daytime UAS operation). The weights that are used to construct PREM from the combination of both layers are 0.4 and 0.6 respectively. Note that, the selection of weights on different layers plays an important role in path characteristics and task-awareness, and therefore, they should be extensively investigated, which is outside the scope of this paper. A higher weight on the risk of flying over traffic might be more realistic in real-life due to the potential cause of catastrophic secondary incidents. Nevertheless, different cases will be demonstrated for the diversity and comparison.

For the selection of start and goal positions, although they can be any two random positions, they are selected to show the effect of various PREMs on the generated paths. Finally, the path planner algorithm is run to find a near-optimal path while continuously exploring the whole map and optimizing the previously found paths at the same time.

Results of the RRT run with above parameters are shown in Fig.(7). The solid red lines in Figs.(7(a)-7(b)) are the final paths for the first and second cases after 10000 iterations, whereas, the blue dashed lines are the paths found during the previous iterations. In the first case, since there is no traffic present in the map, reaching the goal position by traveling over the streets gives the lowest risk path as expected. However, in the second scenario, having a traffic activity on the streets changes the underlying risk map, and it drives planner algorithm to look for the alternative paths to minimize the total risk until reaching the goal. Comparing the first case, the gaps between buildings, without street intersections, and the property backyards give the lowest risk path in Fig.(7(b)). This means that flying over traffic accumulates a higher risk in total than flying near the buildings, as it is decoded in PREM construction. Also note that, for selected ground impact shapes and distributions, the regions that potentially accumulate low risks can easily differ from those selections. For instance, a constant wind flow from one direction over the region would shift the impact domain in the same direction, and it might result in having the lowest risk path that goes above buildings. Therefore, path characteristics for the missions depend on both the underlying risk conditions (PREM) and the vehicle's failure mode representation with environmental effects.

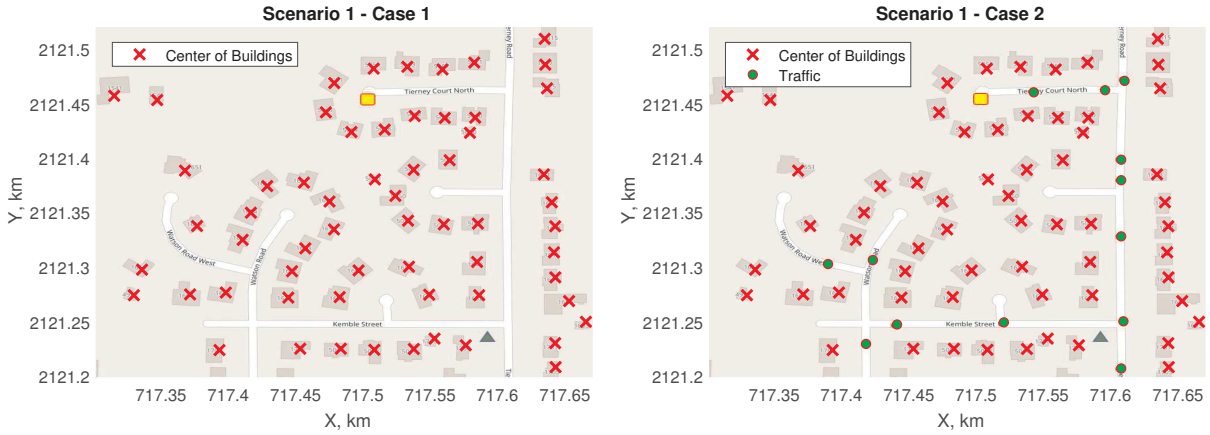

(a) 1st Scenario Map - Case 1

(b) 1st Scenario Map - Case 2

Figure 6. Case maps for the first scenario

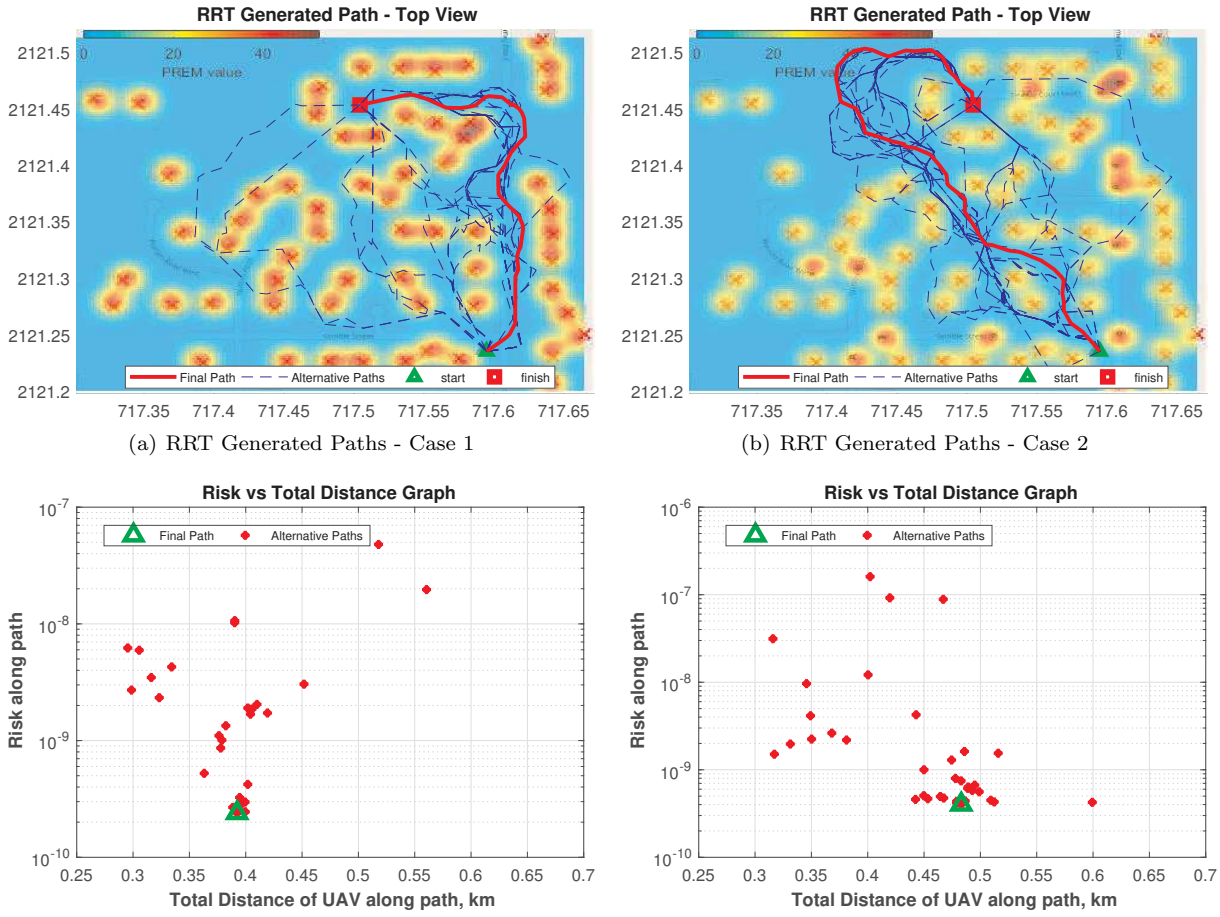

(a) RRT Generated Paths - Case 1

(b) RRT Generated Paths - Case 2

(c) Risk Levels vs Total Distance Chart - Case 1

(d) Risk Levels vs Total Distance Chart - Case 2

Figure 7. Comparing two cases for a UAS mission path under different risk conditions - Scenario 1

As it can be seen from the figures, many alternative paths are found and optimized during the iterations as well, which are plotted in Figs.(7(c)-7(d)). Looking at the risk versus total distance charts, one can decide whether the mission is in acceptable risk limits or within the vehicle's range. Also, information about

the environment, underlying risk regions, and potential paths can be inferred from these charts during the planning process. For example, the convergence rate of the planning can be learned and used to make the decisions for concluding the search, or even, for ruling out some of the map regions.

Moreover, as it can be noticed that some of the very first paths found have long straight edges, which indicates that the RRT has not explored those regions fully yet. As the process advances, those straight lines are optimized on the tree by rewiring to minimize the total risk along the path, and they usually turn into the curly path segments which yield the low-risk levels due to the selection of the risk representations.

Changing the weights on the risk layers, adding/removing layers or modifying ground impact distributions would have altered the search areas for potentially less risky pathways. In the next scenario, the effect of adding a new risk layer on the path planning in a larger map will be analyzed.

B. Second Scenario

In this scenario, comparing the previous one, a larger and more crowded area, where the dimensions are 900 by 900 meters again in Fort Worth, TX, is chosen for the UAS operation. As in the previous scenario, two cases will be investigated in the same map, depicted in Figs.(8(a)-8(b)). However, in addition to property and traffic risk exposure in the first scenario, the third risk layer corresponding to the bystander risk exposure is added in the second case of this scenario. The weights to construct PREM from these three layers are 0.4, 0.4 and 0.2 for the risk of flying over bystanders, traffic and property on the ground respectively. Thus, it is expected to be observed that the UAS path will try to stay as far as possible from the bystanders and the traffic comparing the buildings given the selected impact domains for these scenarios.

After constructing the PREM, bi-directional RRT* algorithm with defined parameters in Table 2 is run to find the path between selected start and goal positions by minimizing the accumulated risk over the path during 10000 iterations. One should notice that using the same step size and the maximum iteration number for a larger map might result in less optimized paths with potential straight lines and zigzags. In order for RRT algorithm to find more optimized solutions, it needs to densely cover the configuration space. Despite that, after finding regions that are potentially leading to an optimal solution, local optimization algorithms can be used to increase the efficiency of the optimization, which is not covered in this paper.

Results for both cases are shown in Fig.(9). In the first case, corresponding to the only property risk exposure case, low risk generating valleys on the map concentrate on open grounds, unoccupied lands, and freeways, resulting in finding more paths around these regions. Especially the final path that first goes through the open park and continues on the highway to reach the destination is the expected behavior of the optimal path on this case. Considering the only risk condition of flying over residential units drives the path search toward those regions to stay away from buildings. On the other hand, in the second case with updated PREM by the integration of bystanders and traffic risk layers, path search focuses more on the areas where no bystanders and traffic activity present due to the higher weighting on these layers. Thus, gaps between buildings and unoccupied areas are mainly used to reach the goal.

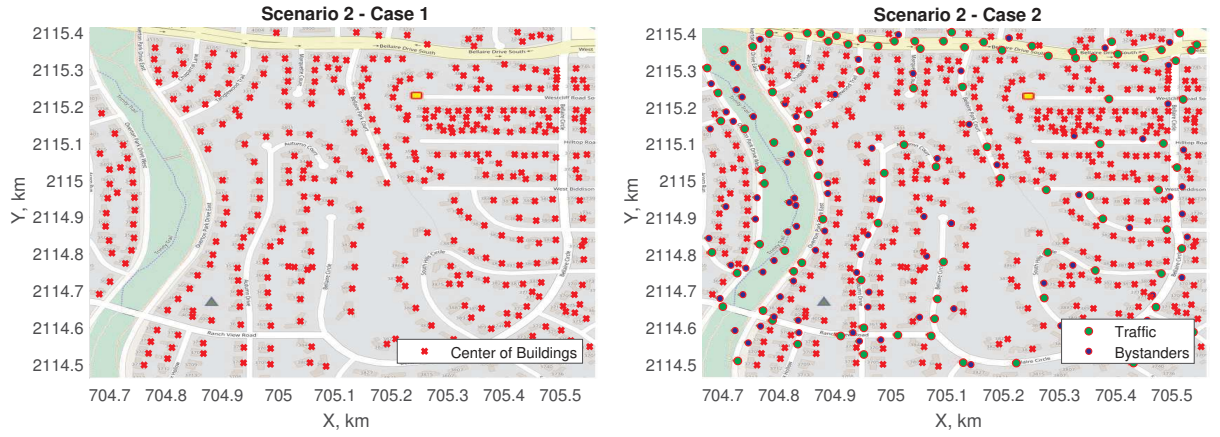

(a) 2nd Scenario Map - Case 1

(b) 2nd Scenario Map - Case 2

Figure 8. Case maps for the second scenario

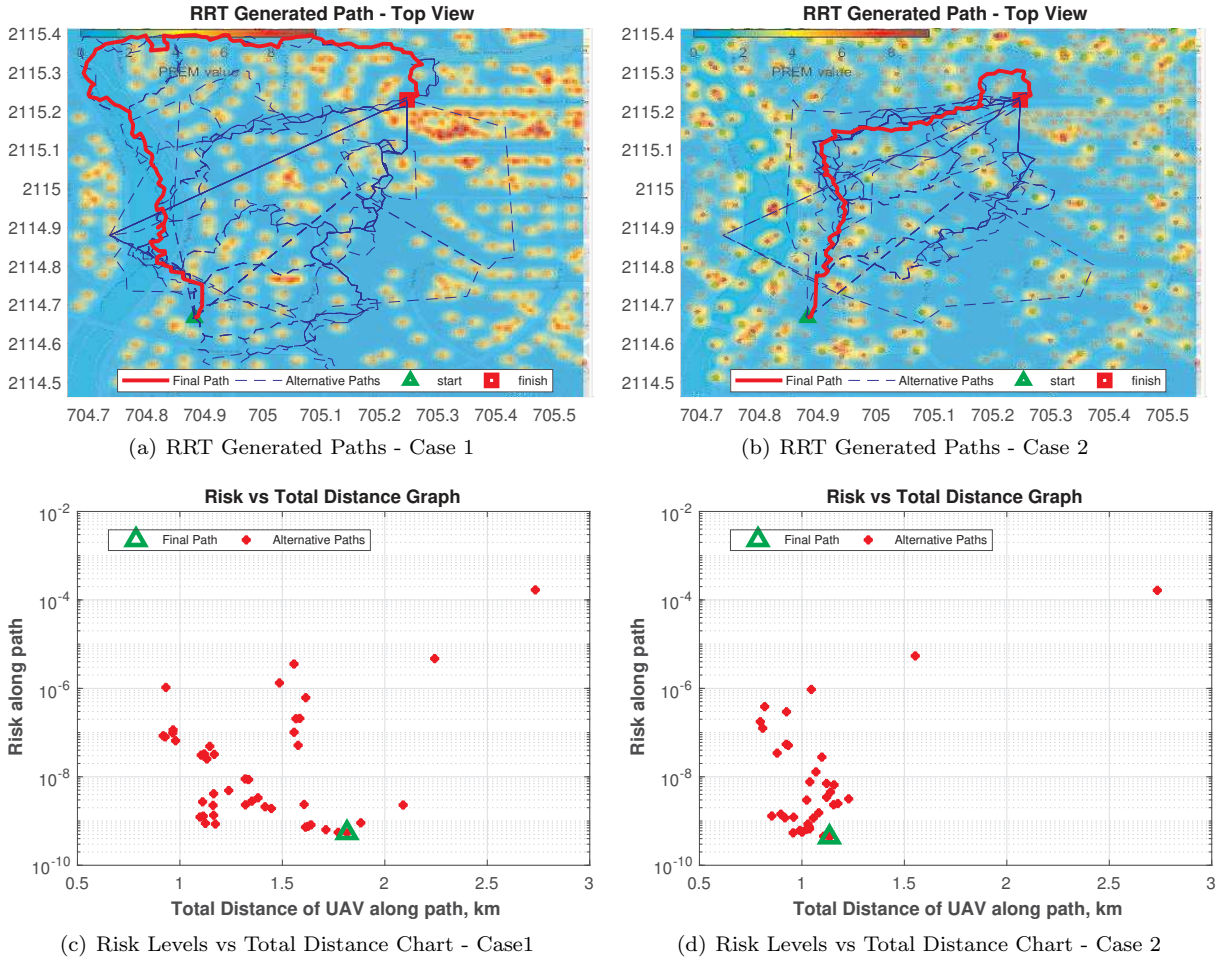

(a) RRT Generated Paths - Case 1

(b) RRT Generated Paths - Case 2

(c) Risk Levels vs Total Distance Chart - Case1

(d) Risk Levels vs Total Distance Chart - Case 2

Figure 9. Comparing two cases for a UAS mission path under different risk conditions - Scenario 2

By this approach, the land use of an area can be used to naturally construct the PREM as one of the most straightforward applications, although the PREM concept has an immensely wider range of integration capabilities. Also, by carefully selecting the relative weights of the risk layers during the construction of the PREM, the task-awareness concept can be implemented into this framework.

VI. Conclusion and Future Works

In this study, a probabilistic risk assessment (PRA) framework is developed to quantify the risk posed by the UAS operations to the ground with the purpose of safe task-aware path planning. First, the probabilistic risk exposure map (PREM) concept is explained and formulated to model the spatial and quantitative distribution of the risk exposures over the map as a mixture of distributions. Then, using the UAS failure mode analysis, ground impact distribution of the platform is represented with a single density function. Finally, the PRA framework is introduced by utilizing the PREM and failure modes to quantify the risk associated with UAS operation to the ground along the planned paths. Introduced PRA framework is implemented into the bi-directional RRT* path planning algorithm to assess the risk of following a path (a cost function), and it is used to compare the paths for different UAS operational scenarios. Results show that various risk conditions can be systematically incorporated into the developed framework to assess and minimize the related risk. Also, the integration of vehicle capabilities and environmental conditions within this framework is a crucial step toward realistic applications. Although only one risk type, which is the risk of being directly hit by a UAS platform, is considered in the scenarios of this study, the flexibility of proposed framework allows various risk types to be addressed as well. In future works, multiple risk

layers corresponding to different risk types, uncertainty on the modeling of PREM, and the effects of vehicle states and environmental conditions on the ground impact distribution will be investigated. Furthermore, in addition to just minimizing the risk along the path, gains for achieving specified goal/subgoals or potentially useful plans such as refueling schedules will be integrated into this framework. Therefore, the planning algorithm will have additional decision criteria to choose among the paths according to their risk and gain comparison. Lastly, another potential improvement can be attained by incorporating Kinodynamic RRT algorithms so that actual vehicle's kinematic and dynamic constraints can be considered during planning.

Acknowledgment

This study is supported by National Science Foundation (S&AS) under the grant 1724248.

References

[1]Bertrand, S., Raballand, N., Viguier, F., and Muller, F., "Ground risk assessment for long-range inspection missions of railways by UAVs," *2017 International Conference on Unmanned Aircraft Systems (ICUAS)*, June 2017, pp. 1343–1351.

[2]Lum, C., Gauksheim, K., Deseure, C., Vagners, J., and McGeer, T., "Assessing and Estimating Risk of Operating Unmanned Aerial Systems in Populated Areas," *11th AIAA Aviation Technology, Integration, and Operations (ATIO) Conference*, Sep 2011.

[3]Aalmoes, R., Cheung, Y. S., Sunil, E., Hoekstra, J. M., and Bussink, F., "A conceptual third party risk model for personal and unmanned aerial vehicles," *2015 International Conference on Unmanned Aircraft Systems (ICUAS)*, June 2015, pp. 1301–1309.

[4]Grimsley, F., "Equivalent Safety Analysis Using Casualty Expectation Approach," *AIAA 3rd "Unmanned Unlimited" Technical Conference, Workshop and Exhibit, Infotech@Aerospace Conferences*, 09 2004.

[5]Clothier, R., Walker, R., Fulton, N., and Campbell, D., "A Casualty Risk Analysis For Unmanned Aerial System (UAS) Operations Over Inhabited Areas," 2007.

[6]Dalamagkidis, K., Valavanis, K. P., and Piegl, L. A., "Evaluating the risk of unmanned aircraft ground impacts," *2008 16th Mediterranean Conference on Control and Automation*, June 2008, pp. 709–716.

[7]Dogan, A., "Probabilistic approach in path planning for UAVs," *Proceedings of the 2003 IEEE International Symposium on Intelligent Control*, Oct 2003, pp. 608–613.

[8]Zengin, U. and Dogan, A., "Real-Time Target Tracking for Autonomous UAVs in Adversarial Environments: A Gradient Search Algorithm," *IEEE Transactions on Robotics*, Vol. 23, No. 2, April 2007, pp. 294–307.

[9]Rito, G. D. and Schettini, F., "Impacts of safety on the design of light remotely-piloted helicopter flight control systems," *Reliability Engineering and System Safety*, Vol. 149, 2016, pp. 121–129.

[10]Karaman, S. and Frazzoli, E., "Sampling-based algorithms for optimal motion planning," *The International Journal of Robotics Research*, Vol. 30, No. 7, 2011, pp. 846–894.

[11]Jordan, M. and Perez, A., "Optimal Bidirectional Rapidly-Exploring Random Trees," 08 2013.

Appendices

A. Bi-directional RRT* Algorithm Appendix

Algorithm 1: Bidirectional RRT*

Input: $(x_{init}, x_{goal}, IterMax, P_{goal}, P_{connect}, Threshold)$
Output: $E_{path}, r_{path}, \sigma_{path}, T_1, T_2$

$V \leftarrow \{x_{init}, x_{goal}\}$; $E_1, E_2 \leftarrow \emptyset$
$T_1 \leftarrow (x_{init}, E_1)$; $T_2 \leftarrow (x_{goal}, E_2)$
for $i = 1$ *to* $IterMax$ **do**
  $p \leftarrow rand([0, 1])$
  if $p < P_{goal}$ **then**
    $x_{rand} \leftarrow x_{goal}$
  else
    $x_{rand} \leftarrow$ Sample
  $x_{nearest} \leftarrow$ Nearest(T_1, x_{rand})
  $x_{new} \leftarrow$ Extend$(x_{nearest}, x_{rand})$
  if $CollCheck(x_{new}, T_1) == False$ **then**
    $r_{new} \leftarrow$ Risk(x_{new}) + Risk$(\sigma_{nearest})$
    $V \leftarrow V \cup (x_{new})$
    $E_1 \leftarrow E_1 \cup ((x_{nearest}, x_{new}))$
    $X_{near} \leftarrow$ Near(T_1, x_{new})
    $L_{near} \leftarrow \emptyset$
    $E_1 \leftarrow$ Rewire$(x_{nearest}, x_{new}, X_{near}, r_{new}, L_{near}, E_1, T_1)$
    $T_1 \leftarrow$ MaintainTree$(E_1, r_{new}, x_{nearest}, x_{new}, T_1)$
    $x_{connect} \leftarrow$ Nearest(T_2, x_{new})
  $p \leftarrow rand([0, 1])$
  if $p < P_{connect}$ **then**
    $x_{rand_2} \leftarrow x_{new}$
  else
    $x_{rand_2} \leftarrow$ Sample
  $x_{new_2} \leftarrow$ Extend$(x_{connect}, x_{rand_2})$
  if $CollCheck(x_{new_2}, T_2) == False$ **then**
    $r_{new_2} \leftarrow$ Risk(x_{new_2}) + Risk$(\sigma_{connect})$
    $E_2 \leftarrow E_2 \cup ((x_{connect}, x_{new_2}))$
    $X_{near_2} \leftarrow$ Near(T_2, x_{new_2})
    $L_{near_2} \leftarrow \emptyset$
    $E_2 \leftarrow$ Rewire$(x_{connect}, x_{new_2}, X_{near_2}, r_{new_2}, L_{near_2}, E_2, T_2)$
    $T_2 \leftarrow$ MaintainTree$(E_2, r_{new_2}, x_{connect}, x_{new_2}, T_2)$
  if $Dist(x_{new}, Nearest(T_2, x_{new})) < Threshold$
   $\vee\ Dist(x_{new_2}, Nearest(T_1, x_{new_2})) < Threshold$
   $\vee\ Dist(x_{new}, x_{new_2}) < Threshold$ **then**
    $(E_{path}, r_{path}, \sigma_{path}) \leftarrow$ Backtrack$(E_1, x_{new}, E_2, x_{new_2})$
return $(E_{path}, r_{path}, \sigma_{path}, T_1, T_2)$

Algorithm 2: Rewire($x_{nearest}, x_{new}, X_{near}, r_{new}, L_{near}, E, T$)

Input: $(x_{nearest}, x_{new}, X_{near}, r_{new}, L_{near}, E, T)$
Output: E

for $x_{near} \in X_{near}$ **do**
  $r_{near} \leftarrow \text{Risk}(x_{new}) + \text{Risk}(\sigma_{near})$
  $\sigma_{near} \leftarrow \text{AddNode}(x_{near}, x_{new})$
  $L_{near} \leftarrow L_{near} \cup ((r_{near}, x_{near}, \sigma_{near}))$
L_{near}.Sort()
for $((r_{near}, x_{near}, \sigma_{near})) \in L_{near}$ **do**
  if *CollisionFree*(σ_{near}) **then**
    if $r_{near} < r_{new}$ **then**
      $x_{min} \leftarrow x_{near}$
      $E \leftarrow E \setminus ((x_{nearest}, x_{new}))$
      $E \leftarrow E \cup ((x_{min}, x_{new}))$
      break
for $((r_{near}, x_{near}, \sigma_{near})) \in L_{near}$ **do**
  if *Risk*(x_{near}) + *Risk*(σ_{new}) < *Risk*(σ_{near}) **then**
    $x_{oldParent} \leftarrow \text{Parent}(E, x_{near}, T)$
    $E \leftarrow E \setminus ((x_{oldParent}, x_{near}))$
    $E \leftarrow E \cup ((x_{new}, x_{near}))$
return E